Available online at www.sciencedirect.com
ScienceDirect
Fuel 87 (2008) 39–57
FUEL
www.fuelfirst.com

Laminar burning velocity and explosion index of LPG–air and propane–air mixtures

A.S. Huzayyin [a], H.A. Moneib [b], M.S. Shehatta [a], A.M.A. Attia [a,*]

[a] High Institute of Technology, Benha University, Benha, Egypt
[b] Faculty of Engineering-El-Matteria, Helwan University, Cairo, Egypt

Received 12 October 2006; received in revised form 27 March 2007; accepted 3 April 2007
Available online 4 May 2007

Abstract

The determination of burning velocity is very important for the calculations used in hazardous waste explosion protection and fuel tank venting, which has a direct impact on environmental protection. The scope of the present study encompass an extensive study to map the variations of the laminar burning velocity and the explosion index of LPG–air and propane–air mixtures over wide ranges of equivalence ratio ($\Phi = 0.7$–2.2) and initial temperature ($T_i = 295$–400 K) and pressure ($P_i = 50$–400 kPa). For this purpose a cylindrical combustion bomb was developed. The reliability and accuracy of the built up facility together with the calculation algorithm are confirmed by comparing the values of the laminar burning velocity obtained for a standard fuel (propane at normal pressure normal temperature conditions, NPT) with those available in the literature. The burning velocity was determined using different models depending on the pressure history (P–t) of the central ignition combustion process at the minimum ignition energy.

The data obtained for the laminar burning velocity is correlated to $S_L = S_{L0}(T/T_0)^{\alpha}(P/P_0)^{\beta}$ where S_{L0} is the burning velocity at NPT, α and β are the temperature and pressure exponents respectively. The value of β is observed to slightly vary with the equivalence ratio for both fuels. However, propane exhibits higher pressure dependency than that of LPG. The maximum laminar burning velocity found for propane is nearly 455 mm/s at $\Phi = 1.1$, while that for LPG is nearly 432 mm/s at 4.5% fuel percent ($\Phi \approx 1.5$). The maximum explosion index, commonly called the "explosion severity parameter", is calculated from the determined laminar burning velocity and is found to be 93 bar m/s for propane, and nearly 88 bar m/s for LPG.

Keywords: Burning velocity; Explosion index; Constant volume combustion; LPG

1. Introduction

The determination of the characteristics of combustible mixtures has and still attracts the interests of combustion specialists. Special focus is given to particular fundamental properties; namely, the laminar burning velocity, minimum ignition energy, ignition delay period, flammability limits and quenching distance [1]. Their values depend mainly on the fuel type, the mixture strength, the temperature and the pressure.

Three combustion velocities are being defined during flame propagation; the burning velocity, flame speed, and the expansion velocity [2]. The former represents the rate at which the flame front propagates into the unburned gas. The flame speed is the velocity of the flame front relative to a fixed position, while the expansion velocity is the difference between the flame speed and the burning velocity.

The accurate determination of laminar burning velocity of combustible mixtures have received particular attention as being: (i) a basic physiochemical property of the premixed combustible gasses [3], (ii) important in studying flame stabilization, (iii) directly determines the rate of energy released during combustion, (iv) a fundamental parameter that influences the performance and emissions

* Corresponding author. Tel./fax: +20 13 323 0297.
E-mail address: ali_maattia@yahoo.com (A.M.A. Attia).

0016-2361/$ - see front matter © 2007 Elsevier Ltd. All rights reserved.
doi:10.1016/j.fuel.2007.04.001

of the combustion process in many combustion devices [4], (v) needed to understand the laminar flamelet concepts [5,6], (vi) a property that affects the quench layer thickness, ignition delay time and ignition energy of the combustible mixture and (vii) needed to calibrate and validate the chemical reaction mechanisms for combustion simulations of different applications [5].

The methods used for the determination of the laminar burning velocity are classified-in accordance of the flame movement into: (a) stationary methods; where the reactants are introduced into the reaction zone and (b) propagating methods; where the reaction zone is introduced into the reactants. From these methods, the bomb method is selected as (a) it needs small amount of fuel, (b) it simulates the combustion process in SIE, (c) it allows best control over the initial conditions and mixture composition, (d) it is self-consistence and especially suitable for the conditions of high pressure [7,8] and (e) it can provide local values of the burning velocity at each instantaneous value of pressure. The bomb method is however subject to some drawbacks that include lengthy and tedious calculations, the initiation of a spherical flame at minimum ignition energy and the non-adiabatic conditions that exist near the end of burning due to heat transfer to the walls of the bomb. The former could be resolved by adopting fast data processing system, while the second may be insured by proper matching between the spark gap and the spark energy.

In the bomb method, the quiescent combustible mixture is ignited at the center of a rigid volume. Simultaneous records of the rising pressure and photography of the growing spheres of flame are obtained. As the flame in progress, the expansion of the burned gases in a rigid volume causes both pressure and temperature of the unburned gas to increase due to adiabatic compression. This progressively change in the initial conditions of the mixture makes it very difficult to propose a single equation for the calculation of burning velocity. Therefore, it is necessary to establish accurate relations between burning velocity and the pressure rise inside the bomb. The bomb method has been used by many investigators [3,9–19].

The scope of the present work covers three distinctive stages namely:

(i) *Stage I*: To validate the accuracy of the newly developed test facility by comparing the measured values of the laminar burning velocity at different equivalence ratios for propane–air mixtures at NTP with those available in the literature.
(ii) *Stage II*: To extend the data obtained for propane–air mixtures to cover higher range of initial pressure.
(iii) *Stage III*: To investigate the effect of equivalence ratio, initial pressure and initial temperature on the values of laminar burning velocity, maximum explosion pressure, and maximum explosion index for LPG–air mixture. Correlations between variables are derived for both propane–air and LPG–air mixtures.

2. Experimental setup and procedure

A schematic layout of the combustion bomb used in the study is shown in Fig. 1. The combustion bomb is a closed cylindrical chamber that can withstand an internal pressure up to 90 MPa and have an internal diameter of 144.5 mm and length of 150 mm. Its end flanges posses housing for Perspex or quartz glass windows having a view diameter of 30 mm. The bomb is equipped with several ports for gas entry, gas discharge, mounting of bourdon and piezoelectric pressure gauges and ignition spark plug.

To fulfill greater filling accuracy and repeatability, the combustible mixture preparation is performed in a separate cylindrical vessel having an internal diameter of 300 mm and length of 350 mm. Before each test, the bomb is scavenged by compressed air at 10 bar and is then evacuated down to 2.5 kPa. The percentages of the constituents of the specified mixture are based on their individual partial pressures. To ensure accurate doses of the constituents, three capacitive pressure transducers of different ranges are used. The vessel is equipped with a 1/3 hp stirrer fan to ensure adequate mixing prior to the charging process. A waiting period of around 3 min – after the completion of the filling process – is found sufficient to ensure quiescent conditions prior to ignition. The mixture is ignited at the centre of the bomb by twin stainless steel electrodes of 2 mm diameter having a fixed gap nearly of 0.8 mm. The ignition energy is supplied from a specially designed capacitive circuit; giving an output voltage of nearly 85 times the supply value with precise adjustment of the minimum ignition energy.

An external electrical heating circuit is incorporated at the outside surface of the bomb to facilitate uniform heating of the mixture within the bomb to the desired initial temperature of the test.

The electric pulse generated at the moment of spark firing is used to trigger the digital storage oscilloscope that monitors and stores both the pressure versus time signal and the triggering signal. The analog data is converted to digital form via a data acquisition card being plugged into PC. The pressure history is collected at a sampling rate of 31,250 samples/s and saved in EXCEL sheet for later analysis. The mean history for at least three identical runs is used for the calculation of the burning velocity. The combustion products are analyzed for CO_2, CO, O_2 and NO_x using ANAPOL AG-model EU200 exhaust gas analyzer.

3. Thermodynamic equations

In the bomb method, the laminar burning velocity can be determined either by the constant volume (integral approach) or constant pressure (differential approach) technique. Both ways has been proved to yield essentially the same results [2,3]. In the former, the equations are integrated over a finite time, while in the later they are solved at instant time. The constant volume technique utilizes the full advantages of the combustion bomb method, but more

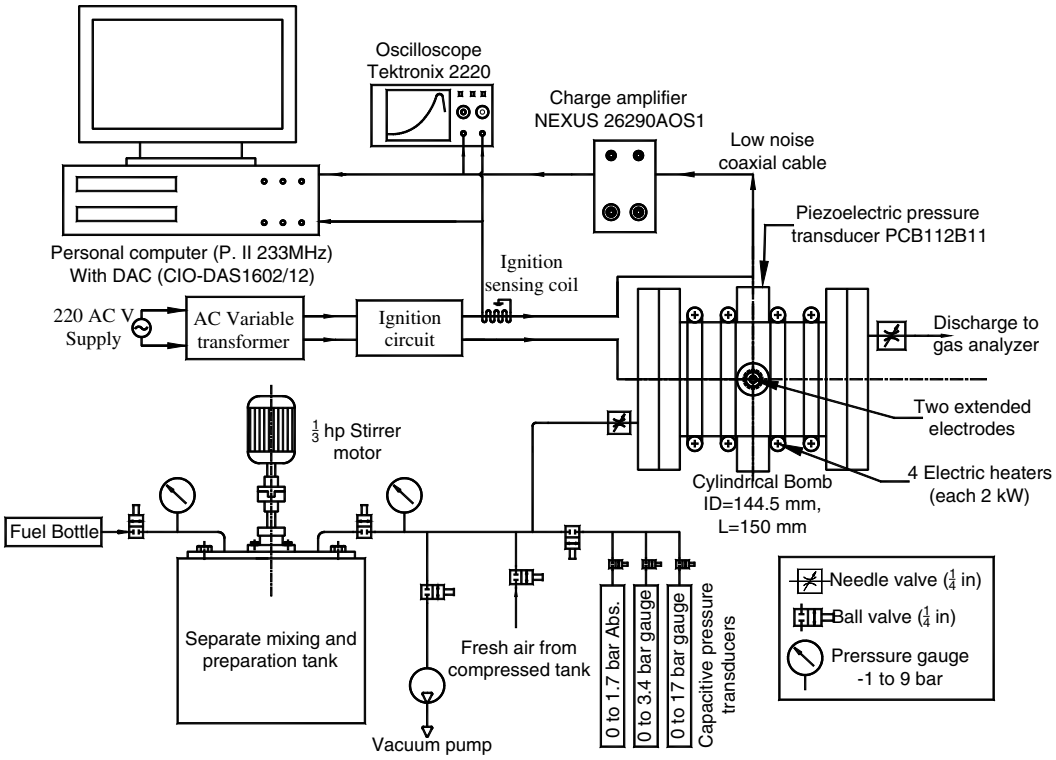

Fig. 1. Layout of the experimental setup.

comprehensive and complicated equations are needed than for the constant pressure technique. The equations needed for both techniques can be derived according to the following assumptions:

(a) An isentropic spherical flame front propagates due to central ignition.
(b) Thin flame thickness or reaction zone; negligible flame thickness this means there is only burned and unburned gases (two zone model).
(c) Adiabatic equilibrium of the burned and unburned gas zone.
(d) The values of burnt gas characteristics (as density and specific heat ratio) behind the flame front can be approximated as average values corresponding to the adiabatic temperature.
(e) Pressure at any instant is uniform throughout the entire volume of the bomb.
(f) Mixture inside the vessel obeys the ideal gas law.

These assumptions are generally considered valid (see detail description by Rallis and Garforth [20]) due to the speed at which the combustion process proceeds.

The constant pressure technique is limited to the pre-pressure period; where the pressure rise does not exceed about 10% of the initial value. Burning velocity can be determined using flame radius record and/or pressure record during the flame propagation inside the bomb throughout the pre-pressure period. This technique was first introduced by Lewis and Von Elbe [9]. Manton et al. [10] developed corroborative equations for the Von Elbe model [9], S_L can be calculated using:

(a) the slope of the flame radius record in conjunction with pressure record [identical to that used by Fiock et al. [21], and
(b) only the flame radius record with the thermodynamically computed value of the equilibrium pressure due to adiabatic constant volume combustion.

Manton et al. [10] concluded that the pressure record is satisfactory to calculate the burning velocity. Another form from model of Lewis and Von Elbe [9] is derived by Bardley and Mitcheson [22] and Dahoe et al. [17]. Bradley and Mitcheson [22] stated their model as universal expression relates pressure rise to the burning velocity as

$$\frac{dP}{dt} = \frac{3S_L\rho_u}{R_s\rho_i}(P_e - P_i)[1 - (P_i/P)^{1/\gamma_u}\{(P_e - P)/P_e - P_i\}]^{2/3} \quad (1)$$

where ρ_u is the density of unburned mixture at the instantaneous combustion process, γ_u is the corresponding specific heat ratio of unburned mixture, P is the corresponding pressure value at instantaneous period during combustion, P_e is the equilibrium end pressure due to constant volume combustion and P_i is the initial pressure.

The whole advantages of the bomb method can be achieved by developing a model from which the burning velocity can be calculated over the whole combustion

process inside the bomb, as the models given by Rallis et al. [11], Babkin and Kononenko [12], Metgalchi and Keck [14,15], Babkin et al. [13], Shebeko et al. [23], Elia et al. [24], and Rahim et al. [25]. The model of Rallis et al. [11] depends on the flame radius and pressure records using either properties of unburned gas, or those of burned gas or combined properties of the unburned and burned gases, which is similar to that introduced by Babkin and Kononenko [12]. However, Metgalchi and Keck [14] used a complex model that depends only on the pressure record during the whole combustion process. They confirm the accuracy of their model by comparing the computed flame radius and its corresponding time with that obtained from a flame cutting a laser beam positioned at a specified point. The model's equations were derived from the energy and the volume balance of burned and unburned zones throughout the combustion process. The solution done to get the mass fraction burned and the product temperature at each reading of uniform pressure.

As pointed in NFPA 68 [26] explosion index (K_G defined as the volume normalization of the maximum rate of pressure rise) varies with test volume. The values obtained for test volume of 1 m^3 is considered as the standard value (ASTM [27]). However if $(dP/dt)_{max}$ is measured in any other test volume, K_G can be estimated by normalization of $(dP/dt)_{max}$ using the cube root of the test volume, hence it is known as cube-root law of K_G [17] as follows: $K_G = (dP/dt)_{max} V^{1/3}$. In this study the value of K_G

Table 1
List of models used in the calculation of burning velocity using a pressure record

Reference	Equations	Comments
Dahoe et al. [17]	$X = \frac{P-P_i}{P_e-P_i}, \quad r_b = r\left(1-\frac{P_iT_uP_e-P}{PT_iP_e-P_i}\right)^{1/3}$ $S_L = \frac{r}{3}\left(\frac{P_i}{P}\right)^{\frac{1}{\gamma_u}}\frac{1}{(P_e-P_i)}\left[1-\left(\frac{P_i}{P}\right)^{\frac{1}{\gamma_u}}\left(\frac{P_e-P}{P_e-P_i}\right)\right]^{-\frac{2}{3}}\frac{dP}{dt}$	Original model was derived by Manton et al. [10] and replaced by that of Dahoe et al. [17] for simplicity of its use and to reduce error in the calculation.
Rallis et al. [11]	$\bar{\beta} = (P/P_i)^{\frac{1}{\gamma_u}}, \quad \bar{\alpha} = \frac{m_b T_e^- P}{m_e T_b P_e}, \quad r_b = r\left(\frac{\beta-1}{\beta-\alpha}\right)^{\frac{1}{3}}, \quad PR = \frac{P}{P_i}$ $X = \bar{\alpha}\left(\frac{\bar{\beta}-1}{\bar{\beta}-\bar{\alpha}}\right), \quad S_L = \bar{\alpha}\left[\frac{dr_b}{dt}+\frac{r_b}{3\bar{\alpha}}\left(\frac{\gamma_u-1}{\gamma_u}\right)\left(\frac{1-\bar{\alpha}}{\bar{\beta}-\bar{\alpha}}\right)\frac{dP}{dt}\right]$	Model uses both P–t and r_b–t record and confirm the accuracy of model by comparing the calculated r_b with the measured one. Value of dr_b/dt is determined from the r_b–t record.
Modified model (2005)	$\frac{dr_b}{dt} = \frac{r}{3}\left(\frac{\bar{\beta}-1}{\bar{\beta}-\bar{\alpha}}\right)^{-\frac{2}{3}}\frac{\left(\begin{array}{l}(\bar{\beta}-\bar{\alpha})\frac{1}{\gamma_u}PR^{\left(\frac{1}{\gamma_u}-1\right)}-(\bar{\beta}-1)*\\ \left(\frac{1}{\gamma_u}PR^{\left(\frac{1}{\gamma_u}-1\right)}-\frac{m_bT_e^-}{m_eT_bP_e}\right)\end{array}\right)}{(\bar{\beta}-\bar{\alpha})^2}\frac{dP}{dt}$ $S_L = \bar{\alpha}\left[\frac{dr_b}{dt}+\frac{r_b}{3\bar{\alpha}}\left(\frac{\gamma_u-1}{\gamma_u}\right)\left(\frac{1-\bar{\alpha}}{\bar{\beta}-\bar{\alpha}}\right)\frac{dP}{dt}\right]$	The model of Rallis et al. [11] is modified in the present work to enable the use of only the P–t record, with the assumption of uniform gas distribution and ignoring the pressure gradient through the unburned mixture; so $\bar{\beta} = \bar{\beta}$
Babkin and Kononenko [12]	$E_i = \frac{M_iT_{bi}}{M_bT_i}, \quad X = \frac{\bar{\beta}+\frac{\gamma_b-1}{\gamma_u-1}\left(1-\bar{\beta}^{1-\gamma_u}\right)-1}{G}, \quad r_b = r(X\bar{\alpha})^{\frac{1}{3}}$ $G = \gamma_b\left[E_i-\frac{\gamma_u}{\gamma_b}\frac{\gamma_b-1}{\gamma_u-1}\right]\bar{\beta}^{1-\gamma_u}+\frac{\gamma_b-\gamma_u}{\gamma_u-1}, \quad \frac{d\bar{\beta}}{dt} = \frac{\bar{\beta}^{\frac{1}{\gamma_u}-1}}{\gamma_uP_i}\frac{dP}{dt}$ $S_L = \frac{r}{3G}\left(\frac{\bar{\beta}+X-1}{\bar{\beta}}\right)^{\frac{1}{3}}\left(\gamma_u+\frac{\gamma_b(1-X)}{\bar{\beta}+X-1}\right)\frac{1}{\bar{\beta}}\frac{d\bar{\beta}}{dt}$	Author gave other forms that use the r–t record and/or P–t record. Many equations to calculate mass fraction burned were introduced that depends on the end pressure
Metghalchi and Keck [15]	$x \cong \frac{P_iv_i}{\gamma_f^o(R_f^oT_f^o-R_uT_u^o)}\left[\frac{P}{P_i}-1-\left(\frac{\gamma_u^o-\gamma_f^o}{\gamma_u^o-1}\right)\left(\left(\frac{P}{P_i}\right)^{\frac{\gamma_u^o-1}{\gamma_u^o}}-1\right)\right]$ $\frac{dx}{dP} = v_i\left[1-(1-x)\frac{v_u}{v_i}\left(1-\frac{\gamma_b}{\gamma_u}\right)+a_\eta+a_b+a_u\right]\Big/\left[\gamma_b(R_bT_b-R_uT_u)\right]$ $r_b = r\sqrt[3]{X\left(\frac{P_i}{P}\right)^{\frac{1}{\gamma_u}}}, \quad S_L = \left(\frac{P_i}{P}\right)^{\frac{1}{\gamma_u}}\frac{r^3}{3r_b^2}\frac{dx}{dP}\frac{dP}{dt}$	The correction for many losses were estimated and found to be not exceed $(0.015X)$ which of neglected effect on (dx/dP) and so on S_L, but these losses were considered in our calculations using derived equation given by authors

obtained directly from the pressure data using the simple equation given by Dahoe et al. [17]:

$$K_G = \left(\frac{dP}{dt}\right)_{max} V^{1/3} = (36\pi)^{1/3}(P_{end} - P_i)\left(\frac{P_{end}}{P_i}\right)^{\frac{1}{\gamma_u}} S_L \quad (2)$$

In the present work, different models are used in the calculation process; they are listed in Table 1. The original form of the model of Rallis et al. [11] used the flame radius and the pressure record. The data of flame radius obtained from the pressure record is compared with that measured by the flame radius record, to validate the accuracy of the model. In the present study model of Rallis et al. [11] is modified to enable the calculation of burning velocity using only the pressure record. The modification is done by differentiating the corroborative equation, and so the burning velocity can be obtained from the P–t record.

4. Calculation method

The Engineering Equation Solver software "EES" [28] is used to perform all the calculations needed due to its superior features over existing numerical equation-solving programs. The pressure–time data and its corresponding derivative are properly smoothed and entered as a parametric table in EES to be solved at each data point (starting from a pressure rise nearly $1.01P_i$ until that corresponding to the inflection point). The program data entry also includes the mixture initial conditions (T_i, P_i and the partial pressure of the mixture's constituents) and the fuel type. The calculation of chemical equilibrium is performed following the CHEM_EQUIL external subroutine as that found in [29]. The results which are obtained at equilibrium conditions include the reactant and product properties; temperature, specific heat ratio, molecular weight, and the mole fraction for each constituent, in addition to the relative and absolute error of pressure reading, pressure rise rate, flame radius, burning velocity, and explosion index. More details in addition to copy of the calculation program are presented by Attia [30].

The reactants properties at any point are determined from the JANAF data table knowing the pressure and the corresponding temperature due to isentropic compression as calculated from the following equation:

$$T_R = T_i\left(\frac{P}{P_i}\right)^{(\gamma_u - 1)/\gamma_u} \quad (3)$$

The product characteristics at any point are determined from the chemical equilibrium due to adiabatic constant pressure combustion process at the pressure reading, that satisfy:

$$H_R(T_R) = H_P(T_P) \quad (4)$$

The thermodynamic properties due to adiabatic constant volume combustion process are determined due to equilibrium to satisfy:

$$U_i = U_e, \quad \text{or} \quad H_i - n_R R_U T_i = H_e - n_e R_U T_e \quad (5)$$

$$P_e = P_i \frac{T_e}{T_i}\frac{n_e}{n_i} \quad (6)$$

As the burned and unburned properties become available, the calculation continue to determine the mass fraction burned, the flame radius, the burning velocity and the explosion index according to the different thermodynamic models listed in Table 1.

5. Experimental program

The entire experimental program is performed according to data listed in Table 2. Propane of purity of 99.91% (with minors of other hydrocarbons) is supplied by the Egyptian National Gas "GASCO" Co. and is used to validate the reliability of the test facility. The domestic usage LPG of has the composition given in Table 3. All runs are performed at the minimum ignition energy. From the pressure–time records, several parameters are derived including the maximum pressure, the maximum rate and duration of pressure rise, the minimum ignition voltage and the ignition delay period. The later is defined as time from the start of ignition until the pressure is just increased to 1% of its initial value.

Table 2
Experimental program

Variables equivalence ratio, Φ	Propane–air from 0.6 to 1.5 with step of 0.1	LPG–air from 0.745 to 2.187
Pressure, P_i	50, 100, 200, 300, and 400 kPa	50, 100, 200, 300, and 400 kPa
Temperature, T_i	305 ± 3 K	294 ± 3, 350 ± 3, and 400 ± 3 K

Table 3
Composition of LPG

Constituents	C_2H_6	C_3H_8	i-C_4H_{10}	n-C_4H_{10}	C_nH_m		$X_{theoretical}$
					n	m	
Present study (2005)	0.04	26.41	26.32	47.22	3.734	9.468	0.0333
Chakraborty et al. [45]	1.4	30.1	25.6	42.1	3.639	9.262	0.0341

6. Experimental results and discussion

6.1. Effect of equivalence ratio

Fig. 2 shows the smoothed pressure histories (P–t) and rate of pressure change (dP/dt) following the ignition of propane–air and LPG–air mixtures at NTP and different equivalence ratio. After successful ignition, the stages of the combustion process exhibit the typical sequence; which starts with an ignition delay period, followed by a pre-pressure period which leads to a steep increase in pressure to a maximum value that indicates the termination of the combustion process. It is then exhibits a steady decline of the both the values of P and dP/dt that signifies heat loss to combustor wall. During the combustion process, the rate of pressure initially increases and reaches its maximum value $(dP/dt)_{max}$ at the inflection point; after which this rate rapidly decreases indicating greater heat loss to the combustor wall as the flame approaches it.

It is evident from Fig. 3 that the values of P_{max}, $(dP/dt)_{max}$, ignition delay period (t_d), total combustion period (t_c) (corresponding to the maximum pressure) are greatly affected by the fuel type and equivalence ratio. Their trends are however similar. When comparing the results for both fuels, the following illustrations and explanations may be given:

1. For a given value of Φ within the flammability limits, the propane air mixtures exhibit faster flame propagation when compared with LPG–air mixtures as indicated by the comparatively higher values or P_{max}, $(dP/dt)_{max}$ and lower values of the delay and combustion times duration; t_c and t_d, respectively. The value of Φ corresponding to the maximum rate of flame propagation is lower ($\Phi = 1.2$) for propane–air when compared to the value ($\Phi = 1.5$) for LPG–air mixture. This is attributed to the differences in the chain-branching and the recombination reaction mechanisms in the two cases [47].
2. For both mixtures, the maximum rate of flame propagation occurs on the rich side since additional fuel is needed to compensate for the effect of dissociation at higher temperature.
3. Slower flame propagations are observed when moving towards the inflammability limits. In the lean side ($\Phi < 1$), part of the energy liberated is consumed by the excess air resulting in lowering the values of P_{max} and $(dP/dt)_{max}$ and rising the values of t_d and t_c. In the rich side ($\Phi > 1$), insufficient oxygen causes incomplete combustion and hence smaller heat liberation.
4. The peak value for NO_x emission is approximately the same for both mixtures, but occurred at different stoichiometry; for propane–air at slightly lean mixture ($\Phi \approx 0.9$) while for LPG–air at rich condition ($\Phi = 1.2$).

For propane, P_{max} occurred at $\Phi \approx 1.2$ that matches found in literature (see [26,46]). However, for LPG, P_{max} occurred at about 4.5% LPG content in air mixture ($\Phi \approx 1.36$) that considered rich condition. In The occurrence of P_{max} at about high rich condition ($\Phi \approx 1.36$) can be owing to combustion mechanism of multi-compound fuels. Comparison of P_{max} and its corresponding differentiation shown in Fig. 4 between the present data and that of Oh et al. [31] for LPG–air mixture shows similar trends for both data of P_{max} and $(dP/dt)_{max}$ which proves the accuracy of our experimental data.

Panel (A) of Fig. 5 shows the variations of the mass fraction burned (x), flame radius (r_b) and laminar burning velocity (S_L) during the combustion process using the different thermodynamic models, previously described in Table 1. The presented results are obtained for a

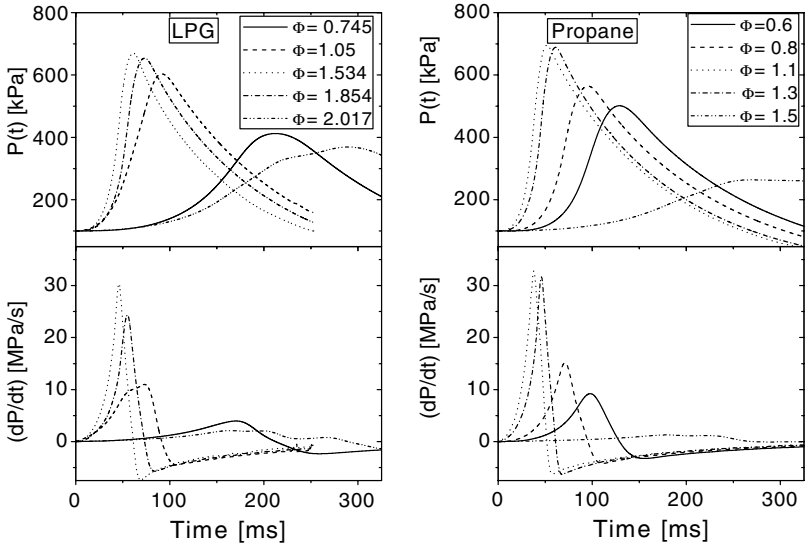

Fig. 2. Samples of pressure histories and corresponding rate of pressure change at different equivalence ratios. [NPT conditions: Panel (a) LPG and panel (b) propane].

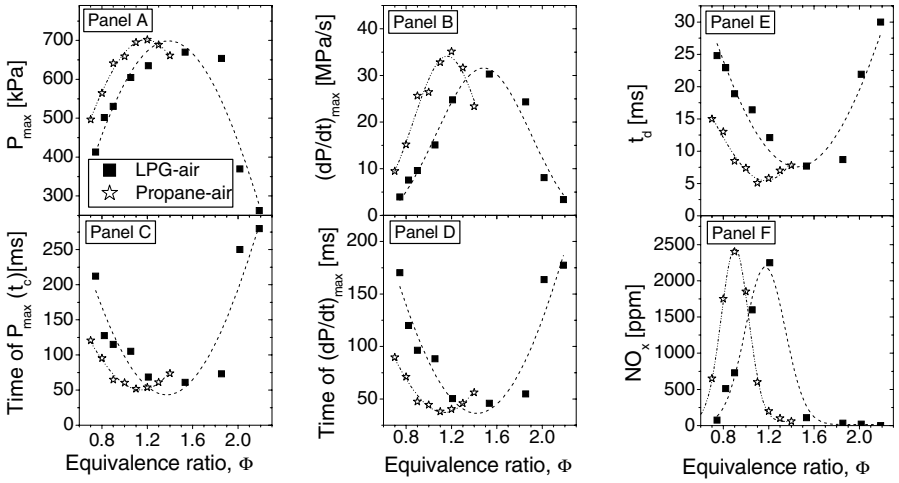

Fig. 3. Different data obtained for both LPG and propane initially at NPT conditions versus equivalence ratios.

propane–air mixture initially at $P_i = 100$ kPa, $T_i = 305$ K and $\Phi = 1.0$, similar behavior but with different values are obtained for LPG–air mixtures. The following conclusion may be withdrawn:

(i) Approximately all models give a linear relation between the mass fraction burned, x and the recorded pressure, P. This verify the simplification of linear relation between x and P used by Manton et al. [10].
(ii) The value of S_L approximately varies linearly with the recorded pressure. This behavior is not only due to pressure effect but mainly due to the isentropic increase in the unburned temperature until a position before the inflection point; where the pressure rise rate begins to fall but is still positive indicating continuing pressure rise.

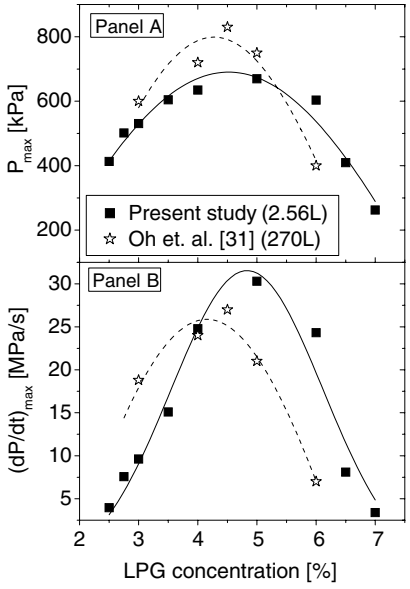

Fig. 4. The maximum explosion pressure compared with that of Oh et al. [31] and the corresponding maximum rate of pressure rise for LPG at NP.

(iii) There existed greater differences between models; with the model of Babkin [12] giving comparatively higher values of x and r_b and lower value of S_L.

The average values of the burning velocities obtained at the pre-pressure period using different models are plotted in Fig. 6. From which it can be observed that, values of S_L calculated based on the model of Manton et al. [10] gives the highest values, while those based on Babkin [12] give the lowest values. While those determined by the present modified model and that of Metghalchi and Keck [15] give close values. The maximum variation of S_L values calculated from different models doe not exceed 15% as deduced from Table 4. The comparison reveals the success of the present modification done for the model of Rallis et al. [11] and the ability to use this modified model for the determination of burning velocity using only the P–t record.

The variations of S_L versus the equivalence ratio for both LPG–air and propane–air mixture at NPT are shown in Fig. 6. It can be noticed that, the maximum value for S_L occurs at Φ prior to that at which the maximum value of pressure occurred. Correspondingly the maximum value of S_L for propane–air mixture take place at $\Phi = 1.1$ for all models tested. The same is observed for LPG–air; S_L occurred at $\Phi \approx 1.4$. The peak of the laminar burning velocity for propane–air mixture (455 mm/s) is slightly higher than that of LPG–air mixture (432 mm/s).

The value of S_L for propane–air mixture at stoichiometric and NPT conditions are calculated by different authors (as shown in Table 5) and its maximum value occurred with the corresponding equivalence ratio are tabulated in Table 5. From Table 5, it can conclude that the present value of S_L at $\Phi = 1$ nearly 415 mm/s is comparable with that deduced by other investigators. In addition there is good agreement for the maximum value of S_L and its stoichiometry; 455 mm/s at $\Phi = 1.1$.

This study make firm the accuracy of the assumption of linear relation between pressure and mass fraction burned whether the model considered is based on constant volume

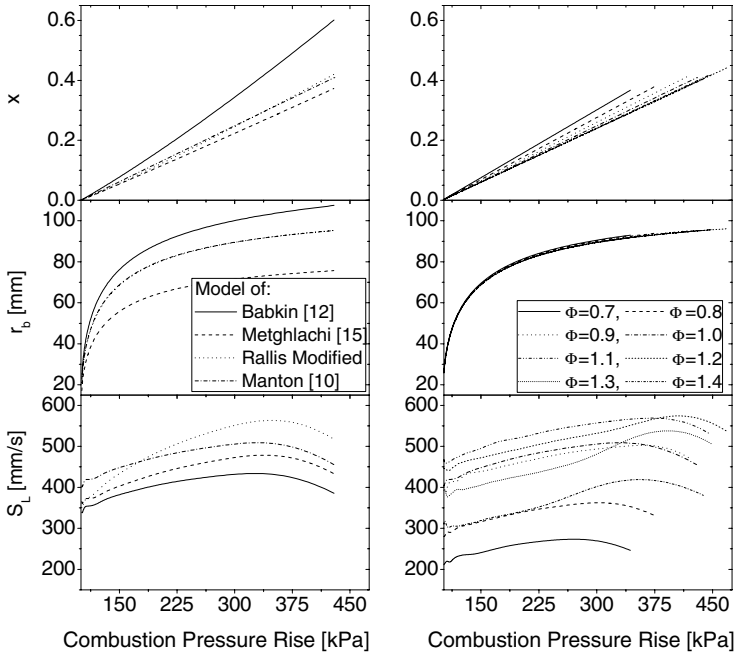

Fig. 5. Mass fraction burned, flame radius, and burning velocity calculated for combustion of propane–air mixture initially at 100 kPa, 305 K, and phi = 1.0 using different models (a), and for various equivalence ratio using Manton et al. [10] model (b).

Table 4
Values of burning velocity calculated for propane–air mixture at NPT using different models and percent of difference relative to those estimated by Manton et al. [10]

Phi Φ	S_L (Manton et al.) (mm/s)	S_L (Metghalchi) (mm/s)	S_L (Rallis) (mm/s)	S_L (Babkin) (mm/s)	$(S_{LV} - S_{LM})/S_{LV}$ (%)	$(S_{LV} - S_{LR})/S_{LV}$ (%)	$(S_{LV} - S_{LB})/S_{LV}$ (%)
0.7	218.14	201.75	201.28	189.40	7.51	7.73	13.18
0.8	287.73	262.59	261.81	247.42	8.74	9.01	14.01
0.9	404.66	364.16	362.93	343.99	10.01	10.31	14.99
1	414.47	369.78	368.51	349.93	10.78	11.09	15.57
1.1	455.42	418.57	417.47	396.51	8.09	8.33	12.93
1.2	445.62	407.55	406.15	385.82	8.54	8.86	13.42
1.3	388.62	359.54	358.40	340.34	7.48	7.78	12.42
1.4	306.69	286.05	285.20	270.60	6.73	7.01	11.77

or constant pressure analysis. This observation agrees with that observed by Stone [18]. Although model of Manton [10] was extremely used through the pre-pressure period analysis, Stone [18] (and others as Dahoe [16,17], Saeed and Stone [32], Clarke et al. [33], and Tanoue [34]) used this model for the whole combustion process until the inflection point of the *P–t* record.

Comparison of the burning velocity for propane–air mixture at NPT is the main verification for the accuracy of the present test facility. For this reason a deep search about most of the available data for propane–air mixture at NPT is performed. Generally, the comparison makes clear the high accuracy of the present test facility for getting reasonable values for propane–air mixture.

Fig. 7 shows different comparisons between the present data for propane–air laminar burning velocity and the corresponding data available in the literature. Comparison include those; (i) using the same model in calculation (panels A and B), (ii) using the same experimental bomb method (panel C), and (iii) using different experimental methods (panel D).

Fig. 7 (panel A) shows comparison between the present data and those obtained by Metghalchi and Keck [14] using the same model in the calculations. Comparison reveals good agreement for both lean and rich sides (with an average relative difference $\leqslant \pm 4\%$), while there are slightly difference for very rich conditions (beyond $\Phi = 1.4$).

In Fig. 7 (panel B) the data calculated by model of Manton [10] or other rearranged form of this model (as that of [22,17]) gives good agreement between the present data and those studies of Tanoue [34], Kido et al. [35], and Desoky et al. [36]. Since Tanoue [34] deduced the unstretched laminar burning velocity, the present data has a slightly lower values at lean side and higher values at higher values. However there is almost agreement for values obtained around the stoichiometry with average of difference over the

Table 5
Overview of burning velocity measured for propane–air mixtures at $\Phi = 1$ and NPT and the maximum value with its corresponding equivalence ratio

Author (year) [Ref.]	Method and technique	S_L (mm/s)	S_{LMax} (at Φ)
Bosschaart and Goey (2004) [43]	Flat burner with heat flux	395	410 (1.1)
Gibbs and Calcote (1959) [42]	Burner tube with apex-cone frustum area using Shadowgraph technique	456	464(1.1)
Dugger and Heimel (1952) [48]	Burner with total area of outer edge of the cone shadow	–	402 (1.05)
Joedicke et al. (2005) [49]	Nozzle burner with Rayligh scattering and laser induced fluorescence facilities	–	492 (1.1)
Zhao et al. (2004) [50]	Single jet-wall stagnation flame	390	395(1.1)
Davis et al. (2002) [44]	Counter flow	418	429 (1.1)
Hassan et al. (1998) [39]	Spherical bomb using r–t record	400	400 (1.1)
Tanoue (2002) [34]	Spherical bomb using r–t record	459.5	467.1 (1.1)
Metghalchi and Keck (1980) [14]	Spherical bomb with P–t record	375	415 (1.1)
Law and Sung (2000) [51]	Counter-Flow, outwardly and inwardly propagation through spherical bomb	425	445 (1.1)
Law and Kwon (2004) [41]	Spherical bomb	387	400 (1.06)
Desoky et al. (1990) [36]	Spherical bomb with P–t record	340	440 (1.2)
Jomaas et al. (2005) [19]	Outwardly spherical bomb with r–t record	415	420 (1.1)
Tanoue (2002) [34]	Modeling	425	434.7 (1.1)
Leung and Lindstedt (1995) [52]	Modeling	470	–
El Bakali et al. (2004) [53]	Modeling	445	470 (1.1)
Zhou and Garner (1996) [38]	Cylindrical bomb with particle image velocimetry	380	405 (1.1)
Senecal and Beaulieu (1998) [46]	Cylindrical bomb with P–t record	–	520 (1.1)
Present study (2005)	Cylindrical bomb with P–t record	Manton et al.: 415	455 (1.1)
		Modified model: 369	418 (1.1)
		Metghalchi-Keck.: 370	419 (1.1)
		Babkin-Kononenko: 350	397 (1.1)

studied range less than ±0.4%, while at the extreme points of $\Phi = 0.8$ and $\Phi = 1.3$ it reaches to ±15%. Kido et al. [35] determined S_L only for lean mixture where $\Phi \leqslant 1$. However, there is a good agreement over the studied range (with difference 15% at $\Phi = 0.7$ and average difference limited to ±4.9%). Data obtained by Desoky et al. [36] shows maximum discrepancy at $\Phi = 1.0$ (nearly −17%), while the overall comparison reveals limited error reaches ±3.6%).

The stretch effect on laminar burning velocity of propane–air mixtures is studied by many authors using flame radius record like Tseng et al. [37], Zhou and Garner [38], Hassan et al. [39], Liao et al. [40], Law and Kwon [41], and Jomass et al. [19]. It is found that, propane–air flames are relatively quick to respond to stretch; stretch decreases the stretched laminar burning velocity for lean mixtures in contrast to increases it for stoichiometric and rich mixtures. Comparison of the present data with those used the bomb method to deduce the unstretched laminar burning velocity is shown in Fig. 7 (panel c). Comparison of the present stretched data with the unstretched data shows good agreement in the lean side until $\Phi = 1.0$. However, present data still has higher values in lean and rich sides.

Comparison of burning velocity calculated from the bomb method in the present study with those obtained from other experimental methods shown in Fig. 7 (panel D), shows accepted agreement especially when the uncertainty of measurements and systematic error associated with each method is considered.

Gibbs and Calcote [42] used the burner method to determine burning velocity for propane–air mixtures and the apex-cone in the calculation with shadowgraph technique for flame photograph. Data obtained by Gibbs and Calcote [42] is relatively high due to the errors associated with the apex and cone angle method.

Zhao et al. [50] used the single jet-wall stagnation flame with PIV to obtain unstretched laminar burning velocity of propane–air mixture, using linear extrapolation to zero stretch rates. Their data found to oscillate about the present data starting from slightly higher value (+10%) at very lean then deceased at stoichiometric and rich mixtures (−15%) with average difference reach to −5%. This oscillation in that manner may be opposed the expected behavior of the unstretched burning velocity but the present discrepancy can be accepted.

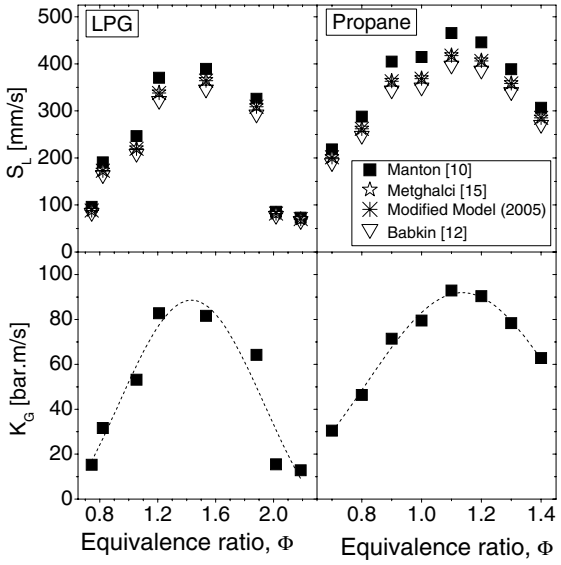

Fig. 6. Burning velocity calculated versus equivalence ratio initially at NPT using different models and the explosion index.

Bosschaart and Goey [43] performed a particular study for flame of hydrocarbons–air mixture stabilized on a honeycomb burner (flat flame method) using the heat flux method. They found that there are a tendency in the heat flux method (and so the flat flame) to produce lower values for burning velocities than the most of other methods; including burner, counter flow, and bomb method. The same result is observed in this study; higher values for all equivalence ratios studied with average difference of 11%.

Davis et al. [44] used the counter flow method in their study of methane- and propane–air combustion to calculate the unstretched laminar burning velocity. Although Fig. 7 (panel D) shows good agreement between the present study and that of Davis et al. [44], while the present data still of higher value in rich side (with overall difference of −8%).

Generally, it can be said that there are good agreement for values of burning velocity for propane–air with the overall data cited in the literature, whatever the method used and better agreement with those deduced from the bomb method. The assets of differences may be due to systematic errors of the experimental data in addition to the uncertainties in the evaluation of burning velocity. However, good agreement between the obtained values indicates the high accuracy of the present test facility and the calculation program, and this confirms the accuracy of data obtained for LPG–air mixtures.

There are limited data in the literature about burning velocity of LPG–air mixtures. However, the obtained values of S_L are considerably higher than that obtained by Chakraborty et al. [45] using the flat flame method, as shown in Fig. 8. Generally, the flat flame method tends to give lower data for S_L as observed by Bosschaart and Goey [43].

Explosion index, K_G versus Φ takes the same trends as that of S_L. The peak value of K_G is an important factor in the risk analysis and is known as gas severity index. K_{Gmax}. For propane–air mixture it is found to be 92 bar m/s, which is being higher than the corresponding values for LPG–air mixture that nearly 83 bar m/s as shown in Fig. 6.

Comparison of the present maximum value of deflagration index, K_{Gmax} for propane–air mixture with those reported in NFPA68 [26] and other should include their

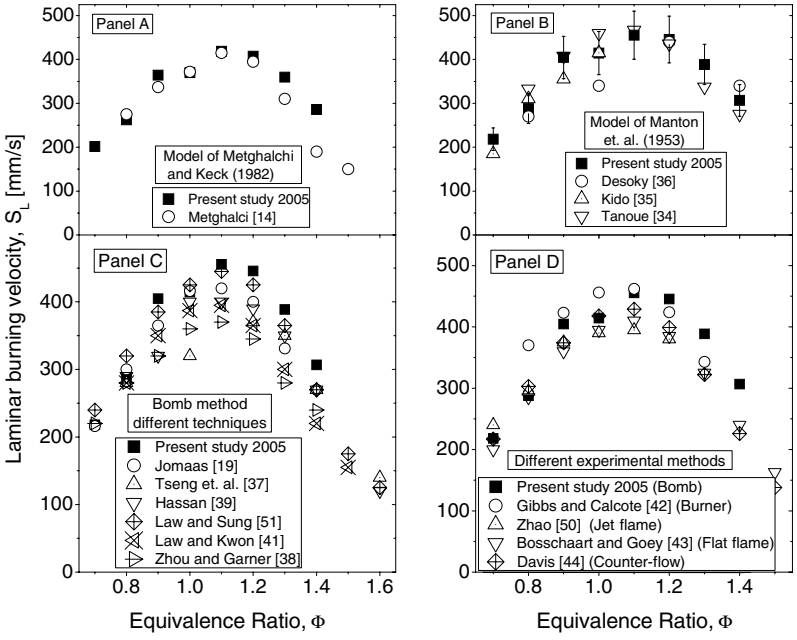

Fig. 7. Laminar burning velocity versus equivalence ratio compared with different data cited in the literature using the same model (panel A and B), the same bomb method (panel C), and other experimental methods (panel D) for propane/air mixture at NPT.

measurement volume and the corresponding value of maximum pressure, P_{max}. Taken into account the confess, that there is no identical K_G values in the literature, because K_G vary with chamber volume and ignition energy even other factors held constant (Dahoe and Goey [16]). Maximum value of K_{Gmax} for propane–air at NPT calculated from 2.56 L cylindrical volume at minimum ignition condition in the present study found to be 93 bar m/s and $P_{max} = 7.02$ bar compared with 100 bar m/s and $P_{max} = 7.9$ bar reported in NFPA68 [26] obtained from 5 L spherical volume using 10 J ignition energy. There is no doubt that the high value of ignition energy affected the value of K_G found in NFPA68 [26]. Senecal and Beaulieu [46] used 22 L cylinder (304 mm I.D. with 350 mm height) to develop K_G data of new interested commercial species; including propane, methane, butane, hydrogen, and other fuels. They estimated the maximum value of K_G for propane–air mixture as 76 bar m/s with $P_{max} = 7.3$ bar, which may be comparable with the present value.

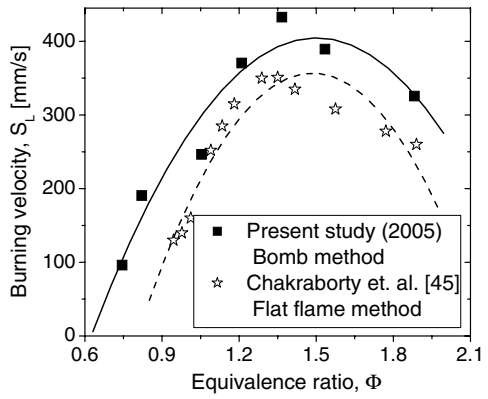

Fig. 8. Comparison between burning velocity in the present study and that of Chakraborty et al. [45] for LPG–air mixtures.

6.2. Effect of initial pressure

Fig. 9 shows the collection of the experimental observations of P_{max}, $(dP/dt)_{max}$ and their corresponding times for propane–air mixture, while those for LPG are shown in Fig. 10. From these figures it can be clearly observed that:

1. As the initial pressure (P_i) increases, the maximum pressure (P_{max}) increases linearly as observed from Fig. 12, due to higher heat liberated resulting from increasing the charge mass. The same behavior is observed for the rate of pressure rise, as P_i increases, $(dP/dt)_{max}$ increases for both fuels. As shown, for LPG–air mixture at $\Phi = 0.745$, mixture cannot be ignited at $P_i = 50$ kPa, which indicates that the lower flammability limit decreases as the initial pressure decreases.
2. For different initial pressure, the peak value of P_{max} occurred at $\Phi = 1.2$ for propane and begins to fall gradually for both rich and lean mixtures for all pressure range studied. The same observation for LPG, but with different numerical values. At elevated pressure higher than atmospheric, P_{atm}, LPG–air mixtures has higher peaks for P_{max} compared with that for propane–air mixtures. Increasing of P_i indicates higher explosion severity.
3. The time of the combustion and that of $(dP/dt)_{max}$ are approximately independent of pressure. This effect is clearer for LPG than for propane, which indicates that propane has higher pressure dependency than LPG. Also, values of t_c and time of $(dP/dt)_{max}$ are observed to be lower in case of propane than those for LPG for all pressure, which confirm the truth of higher flame propagation for propane than for LPG.
4. It can be observed that the time of $(dP/dt)_{max}$ is nearly 60–75% of the total combustion duration (t_c) for each pressure line and for wide ranges of equivalence ratios.

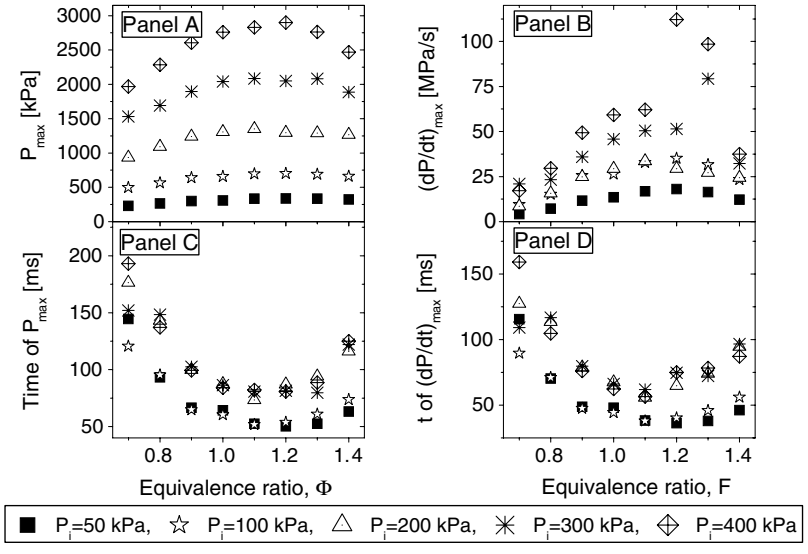

Fig. 9. P_{max}, t_c, $(dP/dt)_{max}$, and time of $(dP/dt)_{max}$ observed experimental for propane–air mixtures versus Φ for different P_i at normal temperature.

5. From Figs. 11 and 12, it can be observed that t_d clearly varies with Φ without unique behavior with the initial pressure. Generally as shown, t_d for both fuels LPG and propane has its minimum value at the atmospheric pressure. Mixtures of LPG–air have higher values of t_d than those for propane–air mixtures for all pressure range studied, which can be attributed to the contents of butane in LPG. For propane–air mixtures there is a peak value for t_d at $P_i = 200$ kPa, while there is two bottoms at $P_i = 100$ kPa and $P_i = 400$ kPa. However, for LPG–air mixtures there is random behavior depending on the mixture strength, but generally as the initial pressure increases the value of t_d increases.

6. Fig. 11 also shows the NO_x formation for both LPG and propane. The peak value of NO_x formation observed at slightly lean mixture for propane–air ($\Phi \approx 0.9$) and at slightly rich mixture for LPG–air ($\Phi \approx 1.1$). The formation of NO_x for LPG increases as P_i increases until P_i reaches 300 kPa then decreases sharply to the minimum values for different equivalence ratios. This effect can be owing to the fact that as P_i increases the adiabatic flame temperature increases that leading to increases of NO_x concentrations. At high pressure ≈400 kPa, the dissociation reactions increase while the reaction rate decreases leading to lower concentrations of NO_x formation. For propane–air mixture NO_x concentration increases with

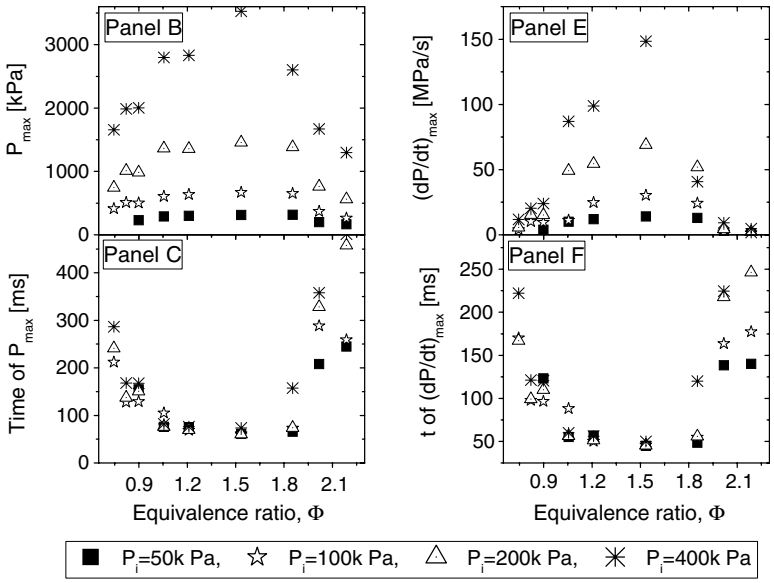

Fig. 10. P_{max}, t_c, $(dP/dt)_{max}$, and time of $(dP/dt)_{max}$ observed experimental for LPG–air mixtures versus Φ for different P_i at normal temperature.

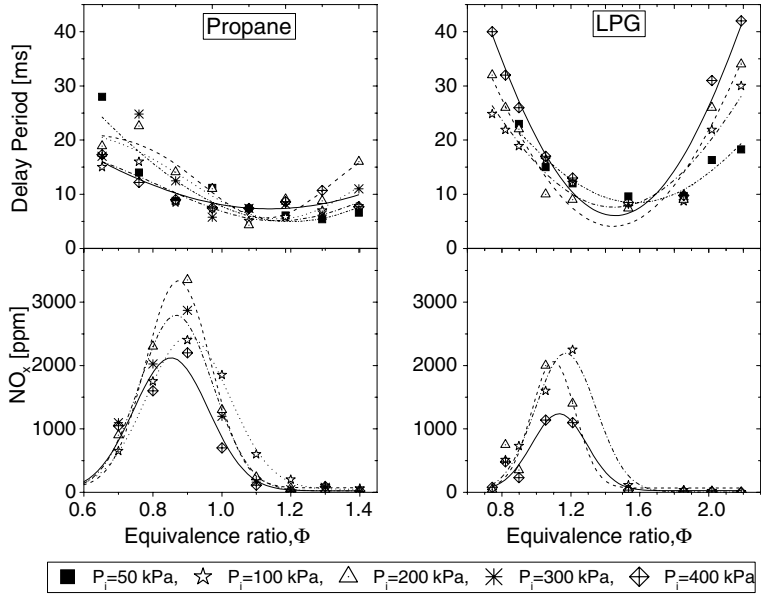

Fig. 11. Delay period and NO_x formation for propane and LPG at normal temperature for different pressure.

initial pressure increases until P_i reaches 200 kPa, after which sharp decreases of NO_x as pressure increases as observed in Fig. 11.

Data of burning velocity obtained for both LPG and propane at different initial pressure is collected in Fig. 13. From Fig. 13 it can be noticed for both fuels that, as the initial pressure increases, the burning velocity decreases. However the rate of decreasing of S_L with P_i for propane–air mixtures is faster than that for LPG–air mixture, which indicates lower dependency of S_L on P_i for LPG–air mixtures. The behavior of the explosion index, K_G, depends on the effects of S_L and P_{max}. This is why explosion index for LPG–air is observed to be lower than that for propane–air at $P_i \leqslant 100$ kPa, then increased to be higher at elevated pressure ($P_i \geqslant 200$ kPa). Because the pressure has a clear effect on S_L for propane–air mixture than for LPG–air mixture, the accumulated effect of P_{max} in addition to the lower pressure dependency give reason why K_G for both fuels have approximately the same peak value at higher pressure ($P_i = 400$ kPa).

Mainly the effects of temperature and pressure on the flame propagation can be explained in terms of the complex kinetic processes that occurred in the flame. As discussed by Glassman [47] for mixtures of $S_L < 600$ mm/s, the pressure exponent varies from 0 to −0.5 while for faster burning mixtures it is zero or slightly positive. Theoretical description of this behavior, can owe the competition between the chain-branching reactions [that has first order pressure sensitivity and very sensitive to temperature] and the recombination reactions [considered not affected by temperature and has a second order pressure sensitivity], Strehlow [29].

Since the burning velocity is lower than 600 mm/s, the competition between chain-branching and recombination reaction, show negative pressure exponent [increase of pressure inhibits the recombination reactions and so temperature variation with pressure for chain-branching reaction will be slight, so S_L decreases as pressure increase]. Which is exactly what is observed from the obtained data for pressure effect for both LPG–air and propane–air combustion. As shown in Figs. 13 and 14, the burning velocity decay as the pressure increases following a power function. Comparison of the burning velocity at various initial pressures with those available in the literature gives accepted agreement as shown in Fig. 14. At $P_i = 50$ kPa the present data show higher values than those of Hassan et al. [39]. The same behavior is observed at $P_i = 400$ kPa. However at $P_i = 200$ kPa and $P_i = 300$ kPa comparison reveals well agreement. At $P_i = 200$ kPa there are well agreement between present data and those of Jomaas et al. [19] and Hassan et al. [39].

6.3. Effect of initial temperature

The initial preheat temperature (T_i) generally enhances the flame propagation rate [47]. Fig. 15 shows sample results of the effect of T_i on the P–t records and dP/dt for LPG–air mixtures at selected values of P_i and Φ. The corresponding variations of P_{max}, $(dP/dt)_{max}$ and t_d with T_i at various values of P_i (50–400 kPa) and Φ (0.82–1.525) are given in Fig. 16.

For the same value of Φ and P_i it is evident that the increase in the value of T_i causes a decline in the value of P_{max} owing to the lower density of the charge that leads to lower mass of the charge burned and hence lower quantity of the heat liberated. The increase in T_i enhances the rate of flame propagation that leads to higher $(dP/dt)_{max}$ and lower delay (t_d) and combustion periods (t_c). It can be noticed that the values of P_{max} and $(dP/dt)_{max}$ are more affected by the initial pressure relative to the initial temper-

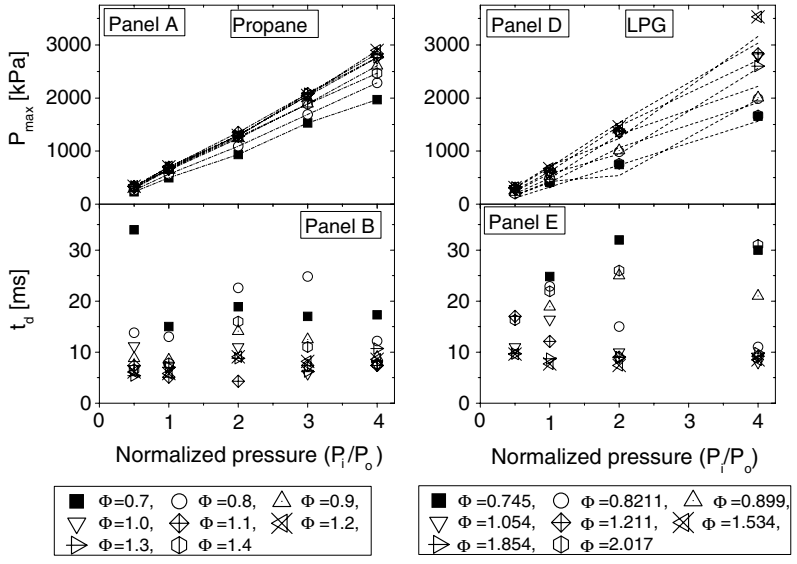

Fig. 12. Maximum pressure and delay period versus normalized initial pressure. Dashed lines represent calculated pressure values using Eqs. (7) and (8).

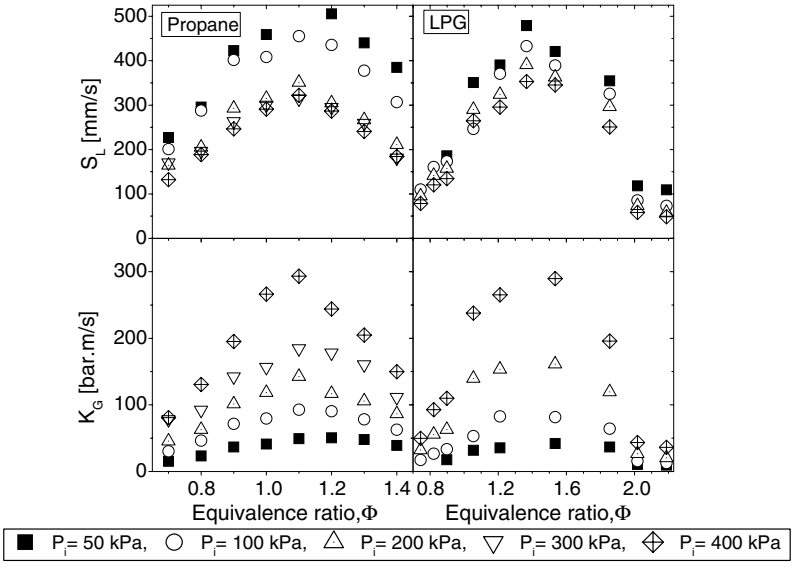

Fig. 13. The laminar burning velocity and explosion index versus Φ at various initial pressures and normal temperature.

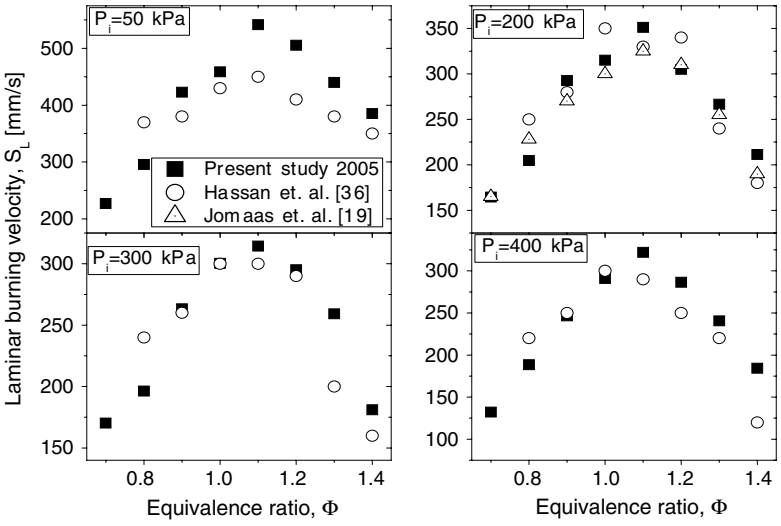

Fig. 14. The laminar burning velocity for propane–air mixtures at various initial pressure and normal temperature compared with available data.

ature. The opposite is true for the variations of t_c and t_d (see Fig. 16).

Fig. 17 shows the variations of NO_x emissions with the value of Φ at three values of T_i (295, 350, 400 K) and two values of P_i (200, 400 kPa). The increase in T_i causes drastic rise in the maximum level of NO_x and a shift of the location of $NO_{x,max}$ to lower values of Φ.

The values of burning velocity, calculated based on the model of Manton et al. [10], are shown in Fig. 18 in addition to the corresponding explosion index. From Fig. 18 it can be observed that, the burning velocity shows a remarkable increase as the initial temperature increase. However, the explosion index show lower dependency on the preheat temperature, due to two opposing effects of lower expansion ratio and the faster burning rate.

The increase of the preheat temperature causes marked increase of the chemical reaction rate and so the flame propagation. In addition to the enhancement effect of the competition of recombination/chain-branching reactions in the preheat zone that leads to strong effect on S_L. This is exactly what is found for the combustion of LPG–air mixture as shown in Fig. 18.

7. The derived correlations

The effect of Φ, P_i, and T_i on P_{max} can be fitted to the following equation; see Fig. 12:

For LPG–air mixtures:

$$P_{max} = -8.3 + (-3424.7 + 10586.5\Phi - 6986.5\Phi^2 + 2203\Phi^3 - 372\Phi^4)(P_i/T_i) \quad (7)$$

where chi-square $R^2 = 0.973$ and standard deviation SD = 131.5

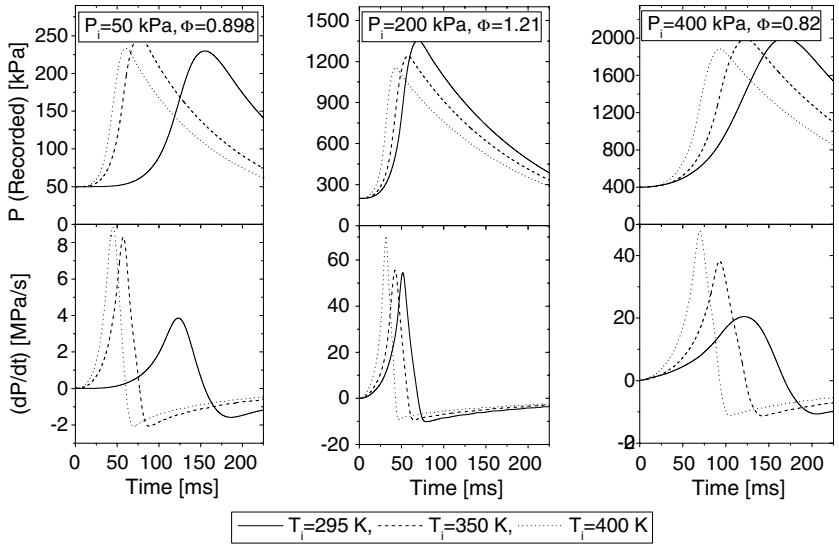

Fig. 15. Samples of the preheat temperature effect on the pressure record and its corresponding pressure rate for LPG–air mixtures at the specified conditions.

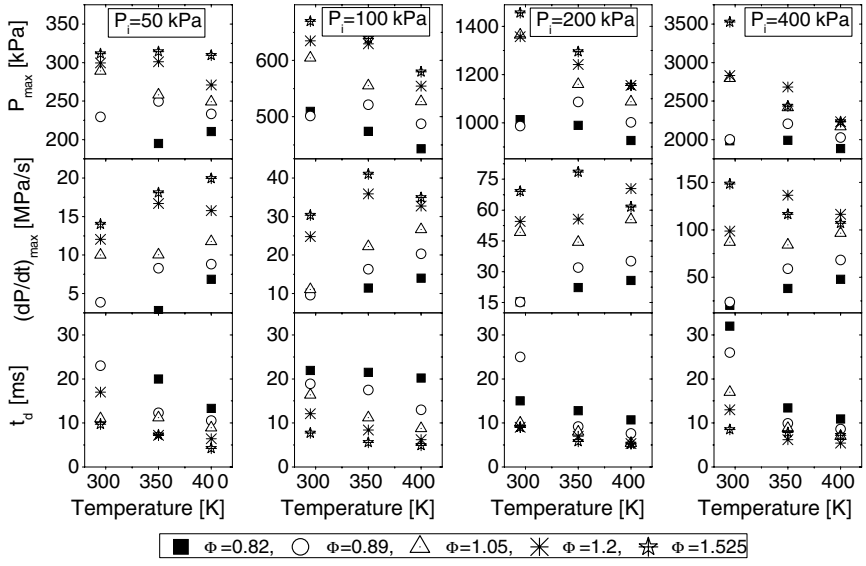

Fig. 16. Samples of the preheat temperature on P_{max}, $(dP/dt)_{max}$, and t_d, for the specified mixtures of LPG–air mixtures.

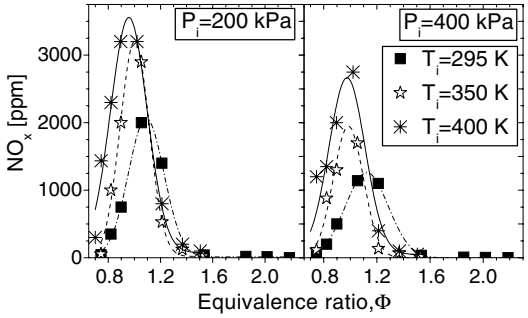

Fig. 17. The effect of initial temperature on NO_x formation.

The equation is valid for:

$0.745 \leqslant \Phi \geqslant 1.9$, $50 \leqslant P_i \geqslant 400$ kPa and $290 \leqslant T_i \geqslant 400$ K

For propane–air mixtures:

$$P_{max} = -26.9 + (-6.2 + 25.6\Phi - 18.7\Phi^2 + 9.4\Phi^3 - 3.26\Phi^4)P_i$$

where $R^2 = 0.998$ and SD = 39.6 (8)

The equation is valid for:

$0.7 \leqslant \Phi \geqslant 1.4$, $50 \leqslant P_i \geqslant 400$ kPa and $T_i = 305$ K

For *LPG–air* the effect of equivalence ratio, initial pressure, and initial temperature on the burning velocity can be fitted as follows (Fig. 18):

$$S_L = S_{L0}(T/T_0)^{\alpha}(P/P_0)^{\beta} \quad (9)$$

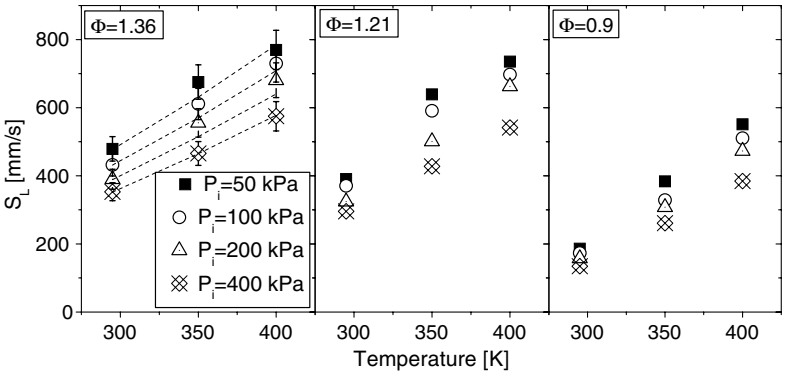

Fig. 18. Variation of S_L with T at different P for LPG–air mixture, points show calculated data and the dashed line at $\Phi = 1.36$ show sample of data extracted from Eq. (9).

where

$$S_{L0} = -492.8 + 1209.1\Phi - 935.5\Phi^2 + 708.1\Phi^3 - 229\Phi^4$$

$$\alpha = 2 + 2.75\Phi - 2.13\Phi^2, \quad \text{and}$$

$$\beta = -0.137 + 0.029\Phi - 0.026\Phi^2$$

The equation is valid for:

$$0.745 \leqslant \Phi \geqslant 1.9, \quad 50 \leqslant P_i \geqslant 400\ \text{kPa} \quad \text{and}$$

$$290 \leqslant T_i \geqslant 400\ \text{K}$$

With SD = 30.57 and $R^2 = 0.972$

For *propane–air* mixture, the obtained data of the burning velocity is fitted to (see Fig. 19):

$$S_L = S_{L0}(P/P_0)^{\beta} \tag{10}$$

where

$$S_{L0} = 5766.8 - 24761.3\Phi + 38798.1\Phi^2 - 25188.3\Phi^3 + 5795.9\Phi^4$$

$$\beta = -0.463 + 0.56\Phi - 0.354\Phi^2$$

The equation is valid for:

$$0.7 \leqslant \Phi \geqslant 1.4, \quad 50 \leqslant P_i \geqslant 400\ \text{kPa} \quad \text{and} \quad T_i = 305\ \text{K}$$

SD = 19.1 and $R^2 = 0.971$

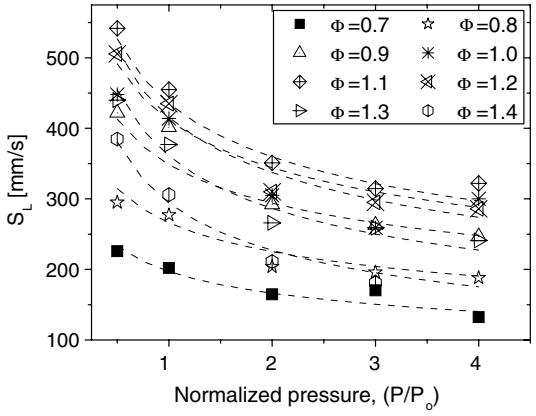

Fig. 19. Variation of S_L with normalized pressure for propane–air mixtures at different equivalence ratio, points represent the calculated data and the dashed line show data extracted from Eq. (10).

The maximum explosion index (commonly called severity index) varies linearly with pressure. For *LPG–air* mixture the variation of the severity index can be fit to temperature and pressure [for T_i varies from 295 to 400 and P_i varies from 50 to 400 kPa], as follows:

$$K_{Gmax} = 8.4 + 0.724P + 0.0394T \tag{11}$$

With SD = 8.35 and $R^2 = 0.99$

While, *for propane*, the obtained data for K_{Gmax}, [that test only for various initial pressure] according to the following equation:

$$K_{Gmax} = 18 + 0.64P \tag{12}$$

With SD = 19.6 and $R^2 = 0.97$

8. Conclusions

The main conclusion from the present study is that, the modification done for the model of Rallis et al. [11] gives an accurate data for the determination of the laminar burning velocity.

However, there are some specific conclusions from the present experimental study according to the experimental observations and the calculations of the burning velocity and explosion index.

(1) For the same P_i, as T_i increases P_{max} decreases while $(dP/dt)_{max}$ increases but the corresponding durations for P_{max} and $(dP/dt)_{max}$ decrease.
(2) At $P_i \leqslant P_{atm}$, P_{max} for propane is higher than that for LPG, while at elevated pressure LPG is higher. The peak value of $(dP/dt)_{max}$ for propane is 20% higher than that for LPG.
(3) The period of inflection point of pressure record are found to be nearly 60–75% of the maximum combustion duration.
(4) Maximum S_L for propane is nearly 455 mm/s, which is considerably higher than that for LPG of approximate 432 mm/s.
(5) As P_i increases, S_L decreases for both fuels, and S_L increases as T_i increases for LPG–air mixture.

(6) K_G increases as Pi increases, but slightly increases as Ti increases.

Appendix A. Error analysis

For an experimental result "R" being computed from a set of N measurements;

$$R = R(X_1, X_2, X_2, \ldots, X_N)$$

The absolute uncertainty in R following the ISO model that utilizes the root-sum-square (RSS) of the individual variables X_i is given by:

$$UR = \sqrt{\sum_{i=1}^{i=N} \left(\frac{\partial R}{\partial X_i} U_{X_i}\right)^2}$$

The relative uncertainty is given by:

$$\frac{UR}{R} = \left[\left(\frac{\partial R}{\partial X_1}\frac{U_{X1}}{R}\right)^2 + \left(\frac{\partial R}{\partial X_2}\frac{U_{X2}}{R}\right)^2 + \cdots + \left(\frac{\partial R}{\partial X_n}\frac{U_{XN}}{R}\right)^2\right]^{\frac{1}{2}}$$

In the uncertainty analysis all partial derivatives were performed using Maple 9.01 (Maple is a complete mathematical problem-solving environment that supports a wide variety of mathematical operations such as numerical analysis, symbolic algebra, and graphics).

A.1. Mixture preparation

Mixture was prepared using partial pressure of its constituents as follows:

$$AF_{\text{actual}} = \frac{P_{\text{air}}}{P_{\text{fuel}}} = \frac{P_{\text{mixture}} - P_{\text{fuel}}}{P_{\text{fuel}}}$$

From which the relative uncertainty in the actual air fuel ratio is:

$$\frac{U(AF_{\text{actual}})}{AF_{\text{actual}}} = \sqrt{\left(\frac{U_{P_{\text{mixture}}}}{(P_{\text{mixture}} - P_{\text{fuel}})}\right)^2 + \left(-\frac{P_{\text{mixture}} * U_{P_{\text{fuel}}}}{P_{\text{fuel}} * (P_{\text{mixture}} - P_{\text{fuel}})}\right)^2}$$

It has its maximum value of nearly ±0.78% at lean conditions ($\Phi = 0.7$) and its minimum value of ±0.38% at rich conditions ($\Phi = 1.5$).

A.2. Initial pressure

In fact, the initial pressure is the sum of the obtained vacuum pressure (measured by Setra280E) and the additional pressure (measured by Setra206 of range 0–3.4 bar) due to charging of the prepared mixture. In this case the relative uncertainty in the initial pressure is calculated as follows:

$$\frac{UP_i}{P_i} = \sqrt{\left(\frac{U_{P_{\text{vacuum}}}}{(P_{\text{added}} + P_{\text{vacuum}})}\right)^2 + \left(\frac{U_{P_{\text{added}}}}{(P_{\text{added}} + P_{\text{vacuum}})}\right)^2}$$

Its maximum value of about ±0.96% occurs at lower initial pressure (50 kPa) and its minimum value of ±0.12% at higher pressure (400 kPa).

A.3. Pressure history

The pressure measured with the piezoelectric pressure sensor and its corresponding numerical differentiation can be considered the major source of error in the uncertainty analysis of the burning velocity calculation. Using the RSS method the uncertainty in pressure reading from sensor (Kistler 6123) is about ±1.118% of the reading. Thus, the relative uncertainty of reading pressure is:

$$\frac{UP}{P} = \pm 0.01118$$

A.4. Pressure differentiation

The numerical derivative of the pressure history is performed according to equation:

$$dP_i(t) = \frac{1}{2}\left(\frac{P_{i+1} - P_i}{t_{i+1} - t_i} + \frac{P_i - P_{i-1}}{t_i - t_{i-1}}\right)$$

The error produced from Data Acquisition (CIO-DAS 1602/12) is ignored. Hence, the relative uncertainty associated with pressure derivative using RSS becomes:

$$\frac{U dP_i}{dP_i(t)} = \pm 2.24\%$$

A.5. Initial temperature

The possible error in the initial temperature comes from two sources namely: (i) the error of the used digital thermometer (±1°K) and (ii) the error due to unavoidable mixture heating by the slightly hot combustion wall bomb which does not exceed ±3°K. Thus, the uncertainty in initial temperature becomes:

$$\frac{UT}{T_i} = \pm\frac{3}{T_i}$$

Note that, generally, if the error from one source exceeds by three times the other, the later is ignored.

A.6. Mass fraction burned

The relative uncertainty in mass fraction burned is:

$$\frac{Ux}{x} = \sqrt{\left(\frac{UP}{P - P_i}\right)^2 + \left(\left(\frac{P - P_i}{P_e - P_i} - 1\right) * \frac{UP_i}{P - P_i}\right)^2}$$

Naturally, it possesses a higher value at the very beginning of the pre-pressure period and decreases to about ±7% as

the pressure rises to $P \approx 1.2P_i$. The average relative uncertainty in x overall the entire pre-pressure period is less than ±12%.

A.7. Flame radius

Using the model of Manton et al. [10] to calculate flame radius, the relative uncertainty in the calculated flame radius can be estimated as follows:

$$fac1 = \frac{1}{3 * \left(\frac{r_b}{r}\right)^3 * (P_e - P_i)} \left(\frac{P}{P_i}\right)^{1/\gamma_u}$$

$$\frac{Ur_b}{r_b} = \sqrt{\left(\frac{Ur}{r}\right)^2 + \left(fac1 * \left(\frac{P_e - P}{\gamma_u P} + 1\right) * UP\right)^2 + \left(fac1 * \left(\frac{P_e - P}{\gamma_u P_i} + \frac{1}{x}\right) * UP_i\right)^2}$$

where *fac1* is a dummy factor.

It is noted that the relative uncertainty in flame radius calculations is less than one-third that of the mass fraction burned. Its average value over the pre-pressure period is about ±6% and about ±2% at $P \approx 1.2P_i$. The value of the relative uncertainty of flame radius varies according to the initial pressure from around ±5% (at 400 kPa) to ±9% (at 50 kPa).

A.8. Burning velocity

The relative uncertainty in the calculation of burning velocity using Dahoe et al. [17] thin flame model can be calculated as follows:

$$fac2 = \frac{1}{(P_e - P_i) - (P_e - P) * \left(\frac{P}{P_i}\right)^{1/\gamma_u}} \left(\frac{P}{P_i}\right)^{1/\gamma_u}$$

$$\frac{US_L}{S_L} = \sqrt{\left(\frac{Ur}{r}\right)^2 + \left(\frac{U dP}{dP/dt}\right)^2 + \left(\frac{-1}{\gamma_u * P} - \frac{2}{3} * fac2 * \left(\frac{P_e - P}{\gamma_u P} + 1\right) * UP\right)^2 + \left(\frac{1}{\gamma_u * P_i} + (1 + fac2) * \frac{P_e - P}{P_e - P_i} * \left(\frac{P_e - P_i}{\gamma_u P_i} + 1\right) * UP_i\right)^2}$$

where *fac2* is a dummy factor.

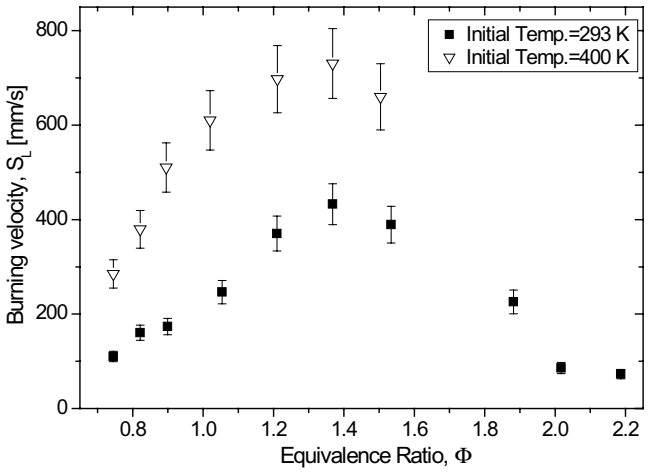

Fig. 20. Burning velocity data with its uncertainty for LPG–air initially at 100 kPa and versus equivalence ratios.

The relative uncertainty in the calculation of laminar burning velocity is less than ±6% at $P \approx 1.2P_i$ with an average of value $\leqslant \pm 10\%$ over the pre-pressure period [for $1.01P_i < P < 1.2P_i$].

Fig. 20 shows the expected error in the calculated burning velocity due to measurements of the pressure history related to LPG–air.

References

[1] Lewis B, Von Elbe G. Combustion flames and explosion of gases. New York: Academic Press, Inc.; 1951.
[2] Ryan TR, Lestz SS. The laminar burning velocity of isooctane, n-heptane, methanol, methane and propane at elevated temperature and pressure in the presence of dilution, SAE 800103, 1980, pp. 652–64.
[3] Rahim F. Determination of burning velocity for methane/oxidizer/diluent mixtures, PhD Thesis, Northeastern University, 2002.
[4] Bayraktar H, Durgun O. Investigating the effects of LPG on spark ignition engine combustion and performance. Energy Convers Manage 2005;46:2317–33.
[5] Hassan MI. Preferential-diffusion/stretch interactions of laminar premixed C/H/O/N flames, PhD thesis, Mechanical Power Engineering, Matteria Faculty of Engineering, Helwan University, Egypt, 1997.
[6] Lipatinkov AN, Chomiak J. Turbulent flame speed and thickness: phenomenology, evaluation and application in multi-dimensional simulations. Progr Energy Combust Sci 2002;28:1–74.
[7] NACA Report No. 1300, National Advisory Committee for Aeronautics, Chapter IV: 1957;321–56.
[8] Bradley D, Hicks RA, Lawes M, Sheppard CGW, Woolley R. The measurement of laminar burning velocities and markstein numbers for iso-octane–air and iso-octane–*n*-heptane–air mixtures at elevated temperatures and pressures in an explosion bomb. Combust Flame 1998;115:126–44.
[9] Lewis B, Von Elbe G. Determination of the speed of flame and temperature distribution in a spherical bomb from time–pressure explosion records. J Chem Phys 1934;2:283–90.
[10] Manton J, Von Elbe G, Lewis B. Burning-velocity measurements in a spherical vessel with central ignition. 4th Symposium (international) on combustion. Baltimore: The Williams & Wilkins Co; 1953.
[11] Rallis CJ, Garforth AM, Steinz JA. Laminar burning velocity of acetylene–air mixtures by the constant volume method: dependence on mixture composition, pressure and temperature. Combust Flame 1965;9:345–56.
[12] Babkin VS, Kononenko YG. Equations for determining normal flame velocity in a constant-volume spherical bomb. Combust, Explosion Shock waves, Translated from Fizika Goreniya i Vzryva 1967;3(2):268–75.
[13] Bankin VS, Bukharov VN, Mol'Kov VV. Normal flame velocity of propane-air mixtures at high pressure and temperature. Combustion, Explosion and Shock waves, Translated from Fizika Goreniya i Vzryva 1989;25(1):57–64.
[14] Metghalchi M, Keck JC. Lamiar burning velocity of propane-air mixtures at high temperature and pressure. Combust Flame 1980;38:143–54.
[15] Metghalchi M, Keck JC. Burning velocities of mixtures of air with methanol, isooctane, and indolene at high pressure and temperature. Combust Flame 1982;48:191–210.
[16] Dahoe AE, Goey LP. On the determination of the laminar burning velocity from closed vessel gas explosions. J Loss Prevent Process Ind 2003;16:457–78.
[17] Dahoe AE, Zevenbergen JF, Lemkowitz SM, Scarlett B. Dust explosion in spherical vessels: the role of flame thickness in the validity of the cube-root law. J Loss Prevent Process Ind 1996;9(1):33–44.

[18] Stone R, Clarke A, Beckwith P. Correlations for the laminar-burning velocity of methane/diluent/air mixtures obtained in free-fall experiments. Combust Flame 1998;114:546–55.
[19] Jomaas G, Zheng XL, Zhu DL, Law CK. Experimental determination of counterflow ignition temperatures and laminar flame speeds of C_2–C_3 hydrocarbons at atmospheric and elevated pressures. Proc Combust Inst 2005;30:193–200.
[20] Rallis CJ, Garforth AM. The determination of laminar burning velocity. Progr Energy Combust Sci 1980;6:303–29.
[21] Fiock EF, Marvin CF, Caldwell FR, Roeder CH. Flame speed and energy considerations for explosions in a spherical bomb, 1940, NACA Report No. 682.
[22] Bradley D, Mitcheson A. A mathematical solution for explosions in spherical vessels. Combust Flame 1976;26:201–17.
[23] Shebeko YN, Tsarichenko SG, Korolchenko AY, Trunev AV, Navzenya VY, Papkov SN, et al. Burning velocities and flammability limits of gaseous mixtures at elevated temperatures and pressures. Combust Flame 1995;102:427–37.
[24] Elia M, Ulinski M, Metghalchi M. Laminar burning velocity of methane–air-diluent mixtures. J Eng Gas Turbines Power, Trans ASME 2001;123:190–6.
[25] Rahim F, Elia M, Ulinski M, Metghalchi M. Burning velocity measurements of methane-oxygen-argon mixtures and its application to extend methane–air burning velocity measurements. Int J Engine Res 2002;3(2):81–92.
[26] NFPA 68, A guide for venting of deflagration, 1998.
[27] ASTM E1226-00, Standard test method for pressure and rate of pressure rise for combustible dusts; 2000.
[28] Kelin SA, Alvarado FL. Engineering equation solver: commercial version 6.883-3D, F Chart Software; 2003 <http://www.Fchart.com>.
[29] Strehlow RA. Combustion fundamentals. New York: McGraw-Hill; 1984, ISBN 0-07-062221-3.
[30] Attia AMA. Burning velocity of combustible mixtures in a cylindrical combustion bomb, M.Sc. Thesis of Engineering and Technology, Mechanical Engineering, High Institute of Technology, Benha University, Benha , Egypt, January, 2006.
[31] Oh K-H, Kim H, Kim J-B, Lee S-E. A study of obstacle-induced variation of the gas explosion characteristics. J Loss Prevent Process Ind 2001;14:597–602.
[32] Saeed K, Stone CR. Measurements of the laminar burning velocity for mixtures of methanol and air from a constant-volume vessel using a multizone model. Combust Flame 2004;139:152–66.
[33] Clarke A, Stone R, Beckwith P. Measurement of the laminar burning velocity of n-butane and isobutane mixtures under micro-gravity conditions in a constant volume vessel. J Inst Energy 2001; 74(September):70–6.
[34] Tanoue K. Turbulent burning velocities of outwardly propagating flames, SAE 2002-01-2842, 2002.
[35] Kido H, Nakashima K, Nakahara M, Hashimoto J. Experimental study on the configuration and propagation characteristics of premixed turbulent flame. JSAE Rev 2001;22:131–8.
[36] Desoky AA, Abdel-gafar YA, El-Badrawy RM. Hydrogen, propane, and gasoline laminar flame development in a spherical vessel. Int J Hydrogen Energy 1990;15(12):895–905.
[37] Tseng LK, Ismail MA, Faeth GM. Laminar burning velocities and markstein numbers of hydrocarbon/air flames. Combust Flame 1993;95:410–26.
[38] Zhou M, Garner CP. Brief communication: direct measurements of burning velocity of propane-air using particle image velocimetry. Combust Flame 1996;106:363–7.
[39] Hassan MI, Aung KT, Kwon OC, Faeth GM. Properties of laminar premixed hydrocarbon/air flames at various pressures. J Propulsion Power 1998;14(4):479–89.
[40] Liao SY, Jiang DM, Gao J, Huang ZH, Cheng Q. Measurements of Markstein numbers and laminar burning velocities for liquefied petroleum gas–air mixtures. Fuel 2004;83:1281–8.
[41] Law CK, Kwon OC. Effect of hydrocarbon substitution on atmospheric hydrogen-air flame propagation. Int J Hydrogen Energy 2004;29:867–79.
[42] Gibbs GJ, Calcote HF. Effect of molecular structure on burning velocity. J Chem Eng 1959;4(3).
[43] Bosschaart KJ, Goey LPH. The laminar burning velocity of flames propagating in mixtures of hydrocarbons and air measured with the heat flux method. Combust Flame 2004;136:261–9.
[44] Davis SG, Quinard J, Searby G. Markstein numbers in counterflow, methane- and propane-air flames: a computational study. Combust Flame 2002;130:123–36.
[45] Chakraborty SK, Mukhopadhyay BN, Chanda BC. Effect of inhibitors on flammability range of flames produced from LPG/air Mixture. Fuel 1975;54:10–6.
[46] Senecal JA, Beaulieu PA. KG: new data and analysis. Process Safety Progr 1998;17(1):9–15.
[47] Glassman I. Combustion. 3rd ed. San Diego: Academic Press; 1996.
[48] Dugger GL, Heimel S. Flame speeds of methane-air, propane-air, and ethylene-air mixtures at low initial temperatures. NACA TN 2624, 1952.
[49] Joedick A, Peters N, Mansour M. The stabilization mechanism and structure of turbulent hydrocarbon lifted flames. Proc Combust Inst 2005;30:901–9.
[50] Zhao Z, Kazakov A, Li J, Dryer FL. The initial temperature and N_2 dilution effect on the laminar flame speed of propane/air. Combust Sci Technol 2004;176:1705–23.
[51] Law CK, Sung CJ. Structure, aerodynamics, and geometry of premixed flamelets. Progr Energy Combust Sci 2000;26:459–505.
[52] Leung KM, Indstedt RP. Detailed kinetic modeling of C_1–C_3 alkane diffusion flames. Combust Flame 1995;102:129–60.
[53] El Bakali A, Dagaut P, Pillier L, Desgroux, Pauwels JF, Rida A, et al. Experimental and modeling study of the oxidation of natural gas in a premixed flame, shock tube, and jet-stirred reactor. Combust Flame 2004;137:109–28.